

## PAPER

CrossMark  
click for updatesCite this: *RSC Adv.*, 2014, 4, 58349

# Amperometric glucose sensor based on boron doped microcrystalline diamond film electrode with different boron doping levels

Yousheng Zou,<sup>\*a</sup> Linlin He,<sup>a</sup> Kang Dou,<sup>a</sup> Shalong Wang,<sup>a</sup> Peiling Ke<sup>b</sup> and Aiying Wang<sup>\*b</sup>

Boron doped microcrystalline diamond (BDMD) films with different boron concentrations were deposited on Si (100) by microwave plasma chemical vapor deposition in a gas mixture of CH<sub>4</sub>/H<sub>2</sub>/TMB. The influence of boron concentration on the surface morphology, microstructure, and electrochemical properties of BDMD film electrodes was studied. It was found that boron dopants play an important role in the structural quality and electrochemical properties of BDMD film electrodes. The increase of doped boron concentration results in the reduction of diamond grain size and the domination of two peaks located at approximately 500 and 1220 cm<sup>-1</sup> in the Raman spectra. Marked differences are observed for BDMD film electrodes with various boron concentrations in impedance characteristics. The electron transfer reaction on BDMD film electrodes becomes faster and reversibility is improved with the increase of boron concentration. Meanwhile, the electrochemical reactions on the BDMD film electrodes become a diffusion controlled process. The non-enzymatic glucose sensors based on as-prepared BDMD film electrodes were developed. The glucose oxidation peak position and current density are dependent on the B/C ratio for the BDMD film electrodes. The results show that appropriate boron doping concentration can improve the conductivity and electrocatalytic activity of BDMD film electrodes. The BDMD film electrode with B/C ratio of 10 000 ppm exhibits the highest sensitivity of 96.88 μA mM<sup>-1</sup> cm<sup>-2</sup>, lowest detection limit of 0.018 mM and widest linear range of 0.1 to 5 mM. The developed non-enzymatic glucose sensors based on as-prepared BDMD film electrodes demonstrate selective detection of glucose in alkaline solution containing interfering species of ascorbic acid and uric acid.

Received 12th September 2014

Accepted 29th October 2014

DOI: 10.1039/c4ra10266e

[www.rsc.org/advances](http://www.rsc.org/advances)

## 1. Introduction

Recently, electrochemical analysis has attracted intensive attention in clinical practice, pollution diagnosis, food industry and biosensing owing to its rapidity, simplicity, low cost, sensitivity and reliability.<sup>1,2</sup> The effect of electrochemical analysis mainly depends on electrode materials including metals, carbon, and ITO. Although noble metals (Au, Pt, Rh) have strong corrosion and oxidation resistance, they are expensive and the intermediate products are easily adsorbed on the electrode surface, which results in the reduction of electrode activity. Carbon materials such as glass carbon, graphite, porous carbon and carbon films have been widely used as electrode materials for electrochemical analysis.<sup>3-5</sup> However, these carbon materials

electrodes have poor stability and are easily contaminated. On the other hand, diamond is the most recent one of the allotropes of carbon to be examined as an electrode material.<sup>6,7</sup> Recently, the boron doped diamond electrode has attracted much interest for electrochemical applications owing to its unique combination of properties, such as wide electrochemical potential window, low background current, superb electrochemical stability in aqueous solution, excellent adsorption resistance as well as good biocompatibility, which outperforms the traditional carbon materials.

Very recently, the glucose sensors have emerged as the key ingredients for the developments of reliable and fast electrochemical analysis. There are two types of electrochemical glucose sensors, with enzyme glucose oxidase (GOx)<sup>8,9</sup> and without oxidase.<sup>10-12</sup> To date, the enzyme glucose sensor with high sensitivity and selectivity to glucose detection has been extensively studied. The enzymatic glucose biosensor using glucose oxidase immobilized onto the graphene and cobalt oxide nanoparticles (Co<sub>3</sub>O<sub>4</sub>-NPs) composite electrode exhibits a wider linear response for glucose from 0.5 mM to 16.5 mM with the sensitivity of 13.52 μA mM<sup>-1</sup> cm<sup>-2</sup>.<sup>8</sup> However, several drawbacks, such as the lack of stability due to the intrinsic

<sup>a</sup>School of Materials Science and Engineering, Institute of Optoelectronics & Nanomaterials, Nanjing University of Science and Technology, Nanjing 210094, China. E-mail: yshzou75@gmail.com; Fax: +86 25 84303279

<sup>b</sup>Key Laboratory of Marine Materials and Related Technologies, Zhejiang Key Laboratory of Marine Materials and Protective Technologies, Ningbo Institute of Materials Technology and Engineering, Chinese Academy of Sciences, Ningbo 315201, China. E-mail: aywang@nimte.ac.cn

nature of enzymes, complicated construction procedures required for the immobilization of enzyme on the electrode surface, and the enzyme activity easily affected by some external factors,<sup>13,14</sup> still remain as the main problems in the practical applications of such sensors. To alleviate the above mentioned drawbacks of enzymatic glucose sensors, numerous studies have been devoted to the investigation and preparation of effective enzyme-free glucose sensors by using various noble metals bimetallic alloys (e.g. Pt, Au, Ni, Pt–Pd and Pt–Au),<sup>11,15–17</sup> oxides (e.g. NiO, Cu<sub>2</sub>O)<sup>18,19</sup> and carbon-based electrodes (e.g. fullerenes, nano-diamond, conducting carbon black nanoparticles, carbon nanotubes and graphene).<sup>12,20–22</sup> The performance of the enzyme-free glucose sensors is mainly dependent on the properties of the electrode materials. Lu *et al.* have reported an enzyme-free glucose sensor with a low detection limit of  $1 \times 10^{-7}$  M and high sensitivity of  $1043 \mu\text{A mM}^{-1} \text{cm}^{-2}$  based on the Ni nanowire arrays electrode, which shows a very high electrochemical active surface area and high electrocatalytic activity for glucose electrooxidation.<sup>23</sup> The non-enzymatic amperometric sensor constructed from graphene nanosheet-wrapped Cu<sub>2</sub>O nanocubes exhibits excellent electrocatalytic activity toward glucose oxidation, high sensitivity and selectivity, and fast amperometric response for the detection of glucose.<sup>24</sup> Zhu *et al.* reported a highly sensitive non-enzymatic amperometric glucose sensor based on CNT/Ni nanocomposite electrode, which exhibits good reproducibility, long-term stability, and high sensitivity of  $1433 \mu\text{A mM}^{-1} \text{cm}^{-2}$ .<sup>25</sup> A novel, stable and sensitive non-enzymatic glucose sensor was developed on Cu–graphene electrode, which presented a wide linear range up to 4.5 mM glucose with a detection limit of 0.5  $\mu\text{M}$  in alkaline solution, high stability and selectivity to glucose.<sup>26</sup>

Boron doped diamond film electrode is considered as an ideal new carbon electrode to be used as electrochemical glucose sensor in recent years.<sup>27–30</sup> Luo *et al.* fabricated the amperometric glucose sensor based on the boron-doped diamond nanorod forest electrode, possessing high sensitivity, selectivity and stability for the potential application in practical glucose detection.<sup>28</sup> A non-enzymatic glucose sensor consisting of a regular array of nickel microdisks on a diamond electrode substrate exhibits a high selectivity for glucose in solutions containing ascorbic and uric acids.<sup>29</sup> Wang *et al.* reported that diamond nanowire electrodes fabricated by a maskless reactive ion etching process with oxygen plasma can be applied for the electrochemical oxidation of glucose without using glucose oxidase, and the detection limit of 60  $\mu\text{M}$  and a linear range up to 8 mM were obtained.<sup>30</sup>

The electrochemical behavior of boron doped diamond film electrode strongly depends on its surface properties such as the grain size, the crystallographic orientation, and boron doped concentration. Moreover, the boron concentration which can considerably modify electrical conductivity and sp<sup>2</sup> carbon content also plays an important role in the boron doped diamond film electrode efficiency. Matsushima *et al.* investigated the influence of boron content on electroanalytical detection of nitrate by using boron doped diamond electrodes and observed a strong dependence between the doping level of the boron

doped diamond film and the nitrate detection.<sup>31</sup> Ndao *et al.* studied the influence of boron concentration in diamond films and observed that only metallic conductive diamond films are efficient for nitrate reduction.<sup>32</sup> Bogdanowicz *et al.* investigated the dependence between the efficiency of oxidants generation and doping level of diamond electrode, and found that higher amounts of dopant on the surface of diamond resulted in the higher efficiency of dye removal in both NaCl and Na<sub>2</sub>SO<sub>4</sub> electrolytes.<sup>33</sup> However, to the best of our knowledge, there were few reports on the effect of boron concentration on the performance of amperometric glucose sensor based on boron doped diamond film electrode. So, complementary studies are justified to correlate the boron doping levels and electrode response for the detection of glucose. In this work we prepared a series of boron doped microcrystalline diamond (BDMD) film electrodes with different B/C ratio in the gas by microwave plasma chemical vapor deposition (MWCVD). The influence of boron doping concentration on the growth characteristic, electrochemical properties and electrochemical detection to glucose were investigated.

## 2. Experimental

### 2.1 Preparation of boron doped microcrystalline diamond film electrode

Boron doped microcrystalline diamond films were prepared on silicon substrate by microwave plasma chemical vapor deposition. Prior to deposition, the surface of silicon wafer was rinsed with alcohol, acetone, deionized water sequentially for 5 minutes to remove impurities. Then silicon substrates were abraded with a suspension liquid of diamond powder (5 nm and less than 0.25  $\mu\text{m}$  mixed) to enhance the nucleation density, the substrates were cleaned again with alcohol and deionized water to remove the diamond powder from the scratches. Methane and hydrogen were used as carbon source and hydrogen source. Trimethyl boron dissolved in the hydrogen was carried into the reaction chamber and used as boron source. The BDMD film deposition was conducted in a gas mixture of 1%CH<sub>4</sub>/99%(H<sub>2</sub> and TMB) with a microwave power of 1200 W and gas pressure of 30 Torr. The boron–carbon (B/C) concentration ratio in the feed gas mixture varied from 8000 to 30 000 ppm. The substrate temperature and deposition time were maintained at approximately 800 °C and 8 h, respectively. The morphology and phase composition of the deposited diamond films were characterized by field emission scanning electron microscopy (SEM, Philips 30 XL FEG) and visible (wavelength: 514.5 nm, Renishaw 2000) Raman spectroscopy.

### 2.2 Chemical and reagents

Glucose (ACS reagent grade), ascorbic acid (ACS reagent grade) and uric acid (ACS reagent grade) were obtained from Sigma-Aldrich and used without any further purification. Potassium ferricyanide (K<sub>3</sub>Fe(CN)<sub>6</sub>, AR grade,  $\geq 99.5\%$ ), potassium chloride (KCl, AR grade,  $\geq 99.5\%$ ) and sodium hydroxide (NaOH, AR grade,  $\geq 96\%$ ) were purchased from Aladdin. The water that was

used in the experiments was ultrapure water (18.2 M $\Omega$  cm) produced by using a simple laboratory water system (Millipore).

### 2.3 Electrochemical measurements

The electrochemical measurements were performed on a CHI660E electrochemical workstation (Shanghai Chenhua, China) in a conventional three-electrode cell system having a BDMD film with different B/C ratio as the working electrode, platinum wire as counter electrode, and a saturated calomel electrode (SCE) as a reference electrode. All experiments were conducted at room temperature. The BDMD film electrodes were washed with deionized water before each electrochemical measurement. Electrochemical impedance spectroscopy (EIS) was performed in an electrolyte solution of 1 M KCl contained 5 mM K<sub>3</sub>Fe(CN)<sub>6</sub>, in a frequency range from 0.1 Hz to 100 kHz with an amplitude of 5 mV. Cyclic Voltammetry (CV) and amperometric *i*-*t* experiments were also carried out.

## 3. Results and discussion

Fig. 1 shows the surface morphology of the prepared BDMD films. It could be seen that the surface morphology changed obviously after the incorporation of boron atoms. From the SEM images, the average grain sizes of the BDMD films were estimated to be about 1.25–1.50, 1.05–1.30, 0.8–1.0 and 0.55–0.8  $\mu$ m for the BDMD film with B/C ratio of 0, 8000, 10 000 and 30 000 ppm, respectively. The grain size of the BDMD films prepared by MWCVD decreased with the increase of boron doping content, which was attributed to excess boron atoms gathered in diamond grain boundary and resulted in formation of structure defects, thus affected the growth of diamond and led to grain refinement. Similar results have also been reported previously.<sup>34</sup> Meanwhile, the feature of twinning bands within the diamond grains is well observed.

Fig. 2 displays the visible Raman spectra of BDMD films grown in different B/C ratio. As to the undoped microcrystalline diamond film, the clear characteristic peak at about 1333 cm<sup>-1</sup> is assigned to sp<sup>3</sup>-hybridized carbon peak. With the increase of

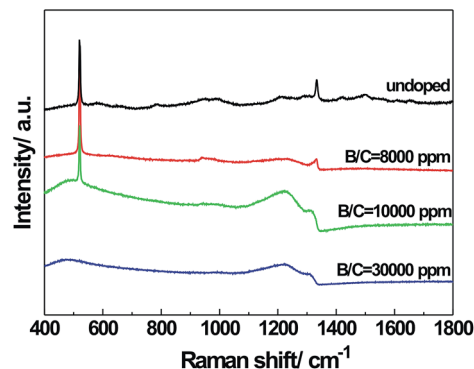


Fig. 2 Visible Raman spectra of BDMD films with various boron doping concentrations.

boron doping concentration, the characteristic diamond peak shifts to lower wave number due to the tensile stress caused by boron doping in diamond films, and the asymmetry of diamond peak becomes more obvious. The drastic changes in spectrum take place at higher boron doping concentration with the appearance of new broad band centered at about 1220 cm<sup>-1</sup>. When the B/C ratio increased to 10 000 ppm, an obvious new peak at about 500 cm<sup>-1</sup> is also present, which is attributed to the concentration increase of the boron pairs. At the B/C ratio of 30 000 ppm, the asymmetry of diamond characteristic peak is further enhanced, and the broad peaks located at around 500 and 1220 cm<sup>-1</sup> become the main features. The asymmetry of diamond characteristic peak and the emergence of the peaks at approximately 500 and 1220 cm<sup>-1</sup> are attributed to the Fano interference caused by quantum mechanics interference between the discrete phonon state and electronic continuum by the presence of boron dopant. The gradual change in the Raman spectra indicates that the microstructure of the BDMD films is affected by boron doping.

Fig. 3 shows the cyclic voltammograms (CVs) of BDMD film electrodes grown in different B/C ratio in 0.4 mM K<sub>3</sub>Fe(CN)<sub>6</sub> with 1 M KCl at different scanning rate. The voltammograms show very well-defined shapes and symmetrical oxidation/reduction peaks. It could be observed that the oxidation peak current and reduction peak current increase with the increase of scanning rate, and the peak current ratio of anodic to cathode is close to 1 for all the BDMD film electrodes. The response current is composed of electrochemical reaction current and electric double layer charging current. The capacitance makes greater contribution to the electric double layer charging current with the increase of scanning rate, which makes the response current increase. The anodic peak potential to cathodic peak potential separations ( $\Delta E_p$ ) for BDMD film electrode increase as the scanning rate increases, which indicates that reversibility deteriorate with the increase of scanning rate. While  $\Delta E_p$  decreases with the increase of boron concentration in microcrystalline diamond at the same scanning rate. The reversibility of the BDMD film electrode with high boron doping level is improved in comparison with low boron doping level, due to the fact that the boron atoms enhance the conductivity of

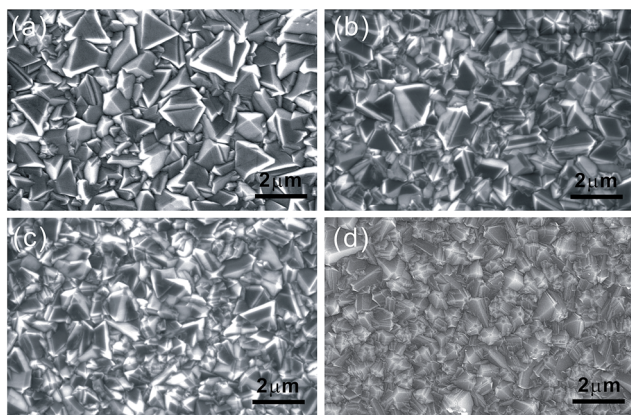


Fig. 1 SEM images of BDMD films with various boron doping concentrations. (a) B/C = 0 ppm, (b) B/C = 8000 ppm, (c) B/C = 10 000 ppm, (d) B/C = 30 000 ppm.

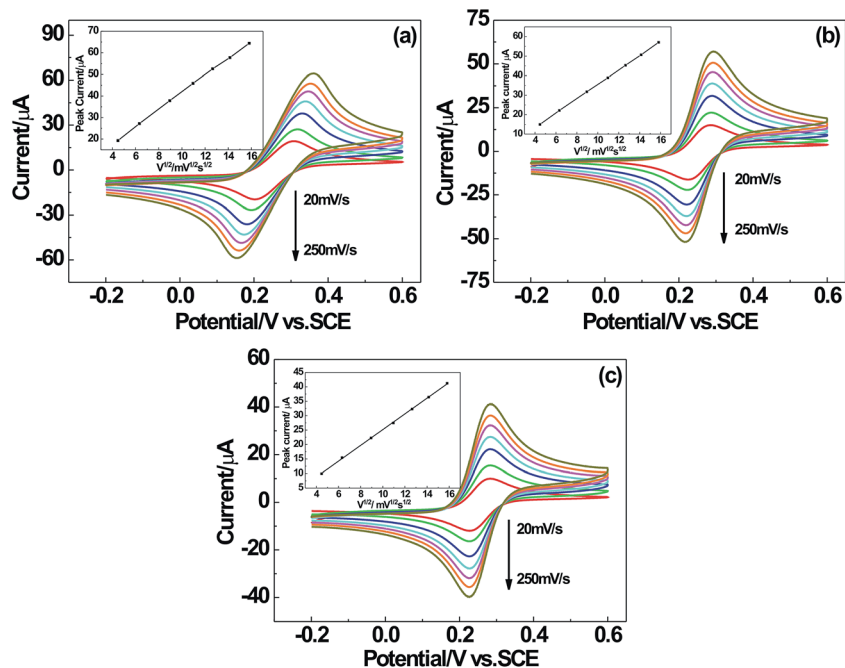


Fig. 3 CVs of BDMD film electrodes with various boron doping concentrations in 0.4 mM  $\text{K}_3\text{Fe}(\text{CN})_6$  with 1 M KCl at different scanning rate. Inset: the relationship between the oxidation peak current and the square root of scanning rate. (a) B/C = 8000 ppm, (b) B/C = 10 000 ppm, (c) B/C = 30 000 ppm.

BDMD film and the charge transfer reaction. The CV results show that the electrochemical properties of BDMD film electrode are affected by boron concentration. The more reversible performance was also observed in the highly boron doped diamond electrode by Azevedo and coworkers.<sup>35</sup> The inset in Fig. 3 demonstrates that the electrochemical response of  $\text{Fe}(\text{CN})_6^{3-/4-}$  on the surface of BDMD film electrode exhibits a linear relationship between the anodic or cathode peak current and square root of scanning rate. This indicates the reactions of ferricyanide ion occurring on the diamond electrode surface are almost reversible and the mass transfer phenomenon in the double layer region of the electrode is mainly controlled by diffusion for all the BDMD film electrodes.

Fig. 4 shows 15 successive CVs of the three BDMD film electrodes grown in various B/C ratio in 0.4 mM  $\text{K}_3\text{Fe}(\text{CN})_6$  with 1 M KCl. The curves are almost overlapped completely after 15 successive measurements for the three electrodes, demonstrating that the diamond electrodes have a good reproducibility without contamination. It indicates that the diamond electrode surface is not poisoned by the reaction intermediates and can be used repeatedly.

Electrochemical impedance spectra (EIS) was applied to study the electrochemical kinetics of BDMD film electrodes, which could give useful information of electron transfer impedance changes on the electrode surface according to the Nyquist plots. A typical Nyquist plot of the impedance spectra includes a semicircular portion at higher frequency corresponding to the electron transfer limited process and a linear portion at lower frequency representing the diffusion controlled process. Fig. 5 shows the EIS of BDMD film electrodes with

various boron doping contents in 1 M KCl electrolyte solution containing 5 mM  $\text{K}_3\text{Fe}(\text{CN})_6$  at the open circuit potential over a frequency range of 0.1 to  $10^5$  Hz. As expected, marked differences are observed for the BDMD film electrodes with various boron concentrations in impedance characteristics. From Fig. 5a, it can be seen that there is only a semicircle appeared at the EIS for the undoped microcrystalline diamond film electrode, indicating that the electrochemical kinetics was very slow and the electrochemical reaction on the diamond electrode

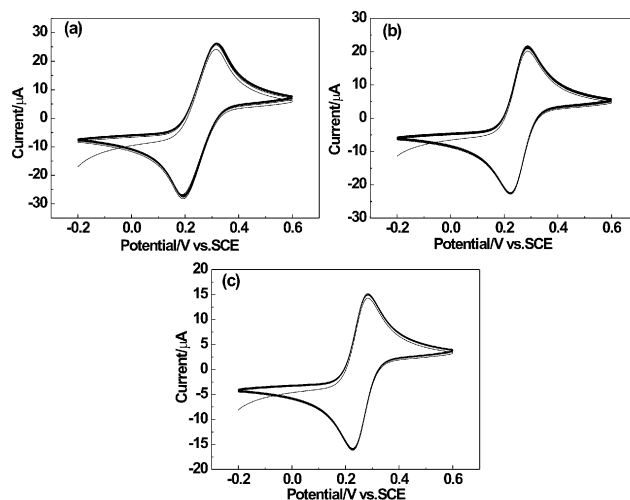


Fig. 4 The fifteen times successive CVs of 0.4 mM  $\text{K}_3\text{Fe}(\text{CN})_6$  in 1 M KCl solution at the scanning rate of  $40 \text{ mV s}^{-1}$  at the BDMD film electrodes with various boron doping concentrations. (a) B/C = 8000 ppm, (b) B/C = 10 000 ppm, (c) B/C = 30 000 ppm.

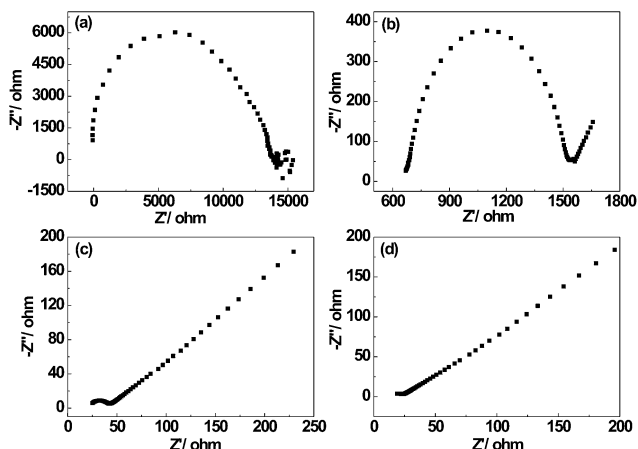


Fig. 5 Nyquist plots of EIS in 5 mM  $K_3Fe(CN)_6$  with 1 M KCl at open circuit potential for BDMD film electrodes with various boron doping concentrations. (a) B/C = 8000 ppm, (b) B/C = 10 000 ppm, (c) B/C = 30 000 ppm.

surface was controlled by electron transfer due to the non-conductivity of the undoped microcrystalline diamond film electrode. However, the effective diameter of the semicircle equaled to electron transfer resistance decreases with the increase of boron doping concentrations, as shown in Fig. 5b–d. This indicates that the electron transfer reaction becomes faster with the increase of boron doping concentration, which is consistent with the results of Fig. 3. As to the Nyquist plots of BDMD film electrode with B/C ratio of 8000, 10 000 and 30 000 ppm, the EIS includes a semicircle and a straight line, which indicates the system was controlled by electrochemical kinetics and diffusion process together. The frequency appeared at diffusion controlled area also reflected the electrochemical reaction rate of the electrodes. The increase of frequency for the BDMD film electrode due to the enhanced conductivity by boron atoms also indicates that the electrochemical kinetics increase with the increase of boron doping concentration. With the increase of boron doped concentrations, the defects in diamond increase, which are in favor of electron transfer. Meanwhile, the energy barrier between BDMD film and electrolyte solutions was reduced after heavily boron-doping, which was advantageous to the electron exchange between the electrode and electrolyte. The results indicate that the incorporation of boron atoms in diamond film significantly increase the electron transfer properties of the BDMD film electrode. The similar results were also observed for boron doped diamond electrode with different boron doping levels by Becker.<sup>36</sup> They investigated the electrochemical impedance spectra (EIS) of boron doped diamond (BDD) electrodes deposited by hot-filament chemical vapor deposition at different doping levels, and observed the activity of BDD depended on the doping level as well as on electrochemical and mechanical treatments of the surfaces. The effective diameter of the semicircle in EIS for BDD (200 ppm) was larger than that of BDD (3000 ppm) by a factor of 70.<sup>36</sup>

Fig. 6 depicts the typical CVs obtained for the BDMD film electrodes with various boron doping contents in 6 mM glucose

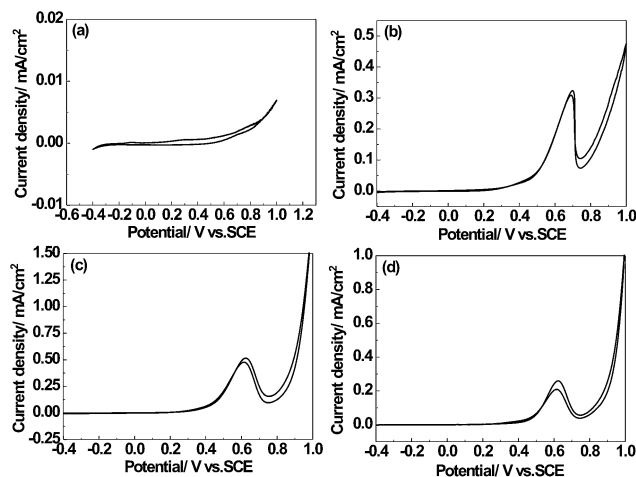


Fig. 6 CVs of BDMD film electrodes with various boron doping concentrations in 6 mM glucose with 0.1 M NaOH at scanning rate of  $30 \text{ mV s}^{-1}$ . (a) B/C = 8000 ppm, (b) B/C = 10 000 ppm, (c) B/C = 30 000 ppm.

with 0.1 M sodium hydroxide solution. The oxidation peak position corresponding to the oxidation of glucose and current density are dependent on the B/C ratio for the BDMD film electrodes. No glucose oxidation peak is observed for the undoped microcrystalline diamond film electrode, while there is an obvious glucose oxidation peak located at 0.690, 0.625 and 0.622 V for the BDMD film electrodes with B/C ratio of 8000, 10 000 and 30 000 ppm, respectively. It suggests that glucose could be readily oxidized on the BDMD film electrodes, and boron atoms may play an important role in the oxidation process of glucose. The oxidation peak potential shifts to negative potential with the increase of boron doping contents, which is related with the improved conductivity caused by boron doping. The glucose oxidation peak current density on the BDMD film electrode surface increases from 0.3083 to 0.5155  $\text{mA cm}^{-2}$  when B/C ratio increases from 8000 to 10 000 ppm. The improved electrical conductivity as well as high surface area resulted from the increase of the grain population density with smaller size is verified justifying the high oxidation peak current density. However, the glucose oxidation peak current density decreases to 0.2595  $\text{mA cm}^{-2}$  when B/C ratio further increases to 30 000 ppm. It demonstrates the higher the boron doping concentrations, the stronger the electro-catalytic ability of BDMD film electrode towards glucose. However, excessive boron concentrations may deteriorate film quality, with clusters of boron and  $sp^2$ -hybridized carbons (amorphous and graphitic carbon) on the surface, resulting in the degradation of electro-catalytic ability. The reproducibility of BDMD film electrodes was also evaluated in 6 mM glucose with 0.1 M sodium hydroxide solution. It was found that the glucose oxidation peak current maintained about 92.4%, 93.1%, 92.7% of their initial peak current values after 15 successive CV measurements for the BDMD film electrodes with B/C ratio of 8000, 10 000 and 30 000 ppm, respectively. This indicated that the non-enzymatic glucose sensor based on BDMD film

electrode was not easy to be contaminated owing to the inertness of the diamond surface.

The reaction mechanism of the oxidation of glucose on boron doped diamond film electrode surface in NaOH solution was discussed as well. It was put forward that boron atoms act as active sites for the glucose oxidation on the BDMD film electrode.<sup>37</sup> Glucose is adsorbed at boron sites on the film electrode surface, and then directly oxidized on the electrode surface. The glucose oxidation peak on the backward sweeping of CVs is almost overlapped to the peak appear on the forward sweep, which indicates that the BDMD film electrode has strong pollution resistance. At the same concentration of glucose, the glucose oxidation peak current density is different for the BDMD film electrodes with various boron concentrations. The increase of doped boron concentration provides more active sites, facilitating the electrochemical oxidation of glucose on the diamond electrode surface. However, the excessive boron atoms resulted in the decrease of glucose oxidation peak current, due to bad quality of diamond film and the increase of defects. The BDMD film electrode with B/C of 10 000 ppm shows the best electrochemical oxidation to glucose, which demonstrates that appropriate boron doped contents can improve the quality and electrochemical properties of diamond film.

Fig. 7 shows the typical amperometric response curves of glucose at BDMD film electrode with B/C ratio of 8000, 10 000 and 30 000 ppm at applied potential of 0.65 V. A well-defined, stable and rapid amperometric response can be observed with the successive addition of 30 mM glucose solution in 0.1 M NaOH solution with continuous stirring at 50 s intervals. It is clear that the electrochemical response to glucose at the BDMD film electrode is very fast in achieving a dynamic equilibrium upon each addition of the sample solution within a short time less than 5 s. Compared with the BDMD film electrodes with B/C ratio of 8000 and 30 000 ppm, the BDMD film electrode with B/C ratio of 10 000 ppm yields a relatively higher current response to glucose, and the  $i-t$  curve exhibits clear steps with successive increase of glucose concentration.

The corresponding calibration curve between current response and glucose concentration for the glucose sensors based on BDMD film is shown in Fig. 8. It can be observed that a

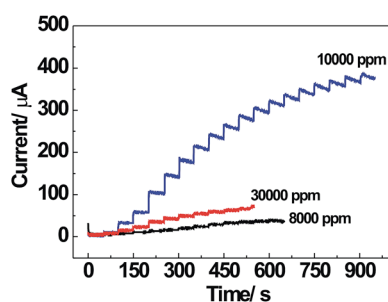


Fig. 7 Amperometric response of BDMD film electrodes with various boron doping concentrations at applied potential of 0.65 V upon successive addition of 30 mM glucose in 0.1 M NaOH with continuous stirring.

much significant current response is obtained at BDMD film electrode with B/C ratio of 10 000 ppm. The glucose sensors based on BDMD film electrode with B/C ratio of 8000, 10 000 and 30 000 ppm display a linear range of 0.1 mM to 2 mM, 0.1 mM to 5 mM and 0.1 mM to 2 mM, and a sensitivity of  $35.44 \mu\text{A mM}^{-1} \text{cm}^{-2}$ ,  $96.88 \mu\text{A mM}^{-1} \text{cm}^{-2}$  and  $29.28 \mu\text{A mM}^{-1} \text{cm}^{-2}$  for glucose, respectively. Meanwhile, the corresponding detection limit with a signal-to-noise ratio ( $S/N$ ) of 3 is 0.04 mM, 0.018 mM and 0.064 mM, respectively. As indicated from the resulting calibration plots, the BDMD film electrode with B/C ratio of 10 000 ppm demonstrates the highest sensitivity and lowest detection limit in comparison with the other two diamond electrodes, which can be attributed to the enhanced electrocatalytic activity, excellent electrical conductivity and large active surface area. This further indicates the proper boron incorporation can improve the quality and electrochemical properties of diamond film electrode. The obtained value of sensitivity from our non-enzymatic glucose sensor based on as-prepared BDMD film electrode with B/C ratio of 10 000 ppm is slightly higher than those given for the non-enzymatic electrochemical glucose sensors based on Pt-Pd nanotube ( $41.5 \mu\text{A mM}^{-1} \text{cm}^{-2}$ ) and nanowire arrays electrodes ( $27.6 \mu\text{A mM}^{-1} \text{cm}^{-2}$ ),<sup>11</sup> Pt/MWCNTs (multi-walled carbon nanotubes) electrode ( $11.83 \mu\text{A mM}^{-1} \text{cm}^{-2}$ ),<sup>38</sup> CuO/TiO<sub>2</sub> nanotube arrays electrode ( $79.79 \mu\text{A mM}^{-1} \text{cm}^{-2}$ ) (ref. 39) and PTAu-MnO<sub>2</sub>/Graphene electrode ( $58.54 \mu\text{A mM}^{-1} \text{cm}^{-2}$ ).<sup>40</sup> However, it is lower than that of  $668.2 \mu\text{A mM}^{-1} \text{cm}^{-2}$  reported for NiO nanoparticles (NPs)/Pt NPs/electrochemically reduced graphene oxide (NiO/Pt/ERGO) ternary composite modified electrode,<sup>41</sup> and  $922 \mu\text{A mM}^{-1} \text{cm}^{-2}$  reported for Cu-MWCNTs nanocomposite electrode.<sup>42</sup> Moreover, the non-enzymatic glucose sensor based on the as-prepared BDMD film electrode with B/C ratio of 10 000 ppm also exhibited a low detection limit of 0.018 mM and wide linear range in 0.1–5 mM, which can be comparable to the values of 0.002 mM and 0.5–7.5 mM reported for the Cu-MWCNTs nanocomposite electrode.<sup>42</sup>

As is well known, ascorbic acid and uric acid are the main interfering species in the detection of glucose, which may be electrochemically oxidized and influence the response of glucose in both glucose oxidase sensor and non-enzymatic glucose sensor. Fig. 9 shows the CVs of BDMD film electrode with B/C ratio of 8000 ppm, 10 000 ppm and 30 000 ppm in 6 mM glucose with interference compounds of AA and UA. The

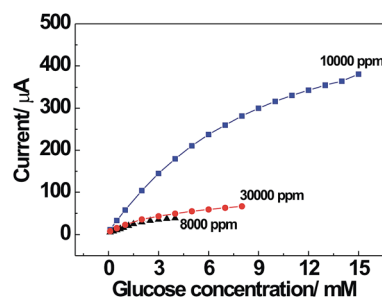


Fig. 8 The calibration curve of current vs. concentration of glucose at BDMD film electrodes with various boron doping concentrations.

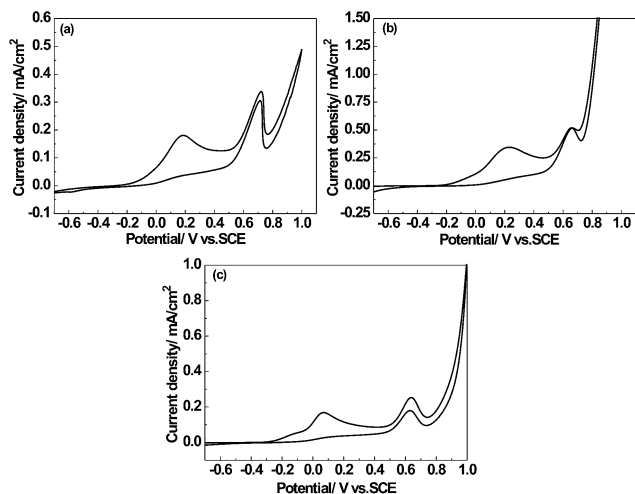


Fig. 9 CVs of BDMD film electrodes with various boron doping concentrations in 6 mM glucose with interference compounds of AA and UA. The supporting electrolyte and the scan rate are 0.1 M NaOH solution and  $25 \text{ mV s}^{-1}$ , respectively.

concentrations of UA and AA were 0.5 mM, which is well above the physiological concentrations of about 0.1 mM. As can be seen, a well-defined glucose response signal can be obtained when coexisted with AA and UA for the three BDMD film electrodes. The oxidation peaks of AA and UA do not overlap with the oxidation peak of glucose. Therefore, BDMD film electrode can be used as an ideal sensor to achieve the selective detection of glucose in the presence of interfering species.

## 4. Conclusions

Boron doped microcrystalline diamond films with B/C ratio of 8000, 10 000 and 30 000 ppm were deposited by MWCVD in a gas mixture of  $\text{CH}_4/\text{H}_2/\text{TMB}$ . The concentration of boron dopant shows remarkable influence on the surface morphology, microstructure, and electrochemical properties of the microcrystalline diamond films. The increase of boron concentration results in the reduction of grain size and degradation of the structural quality of the diamond film. Two new peaks located at approximately  $500$  and  $1220 \text{ cm}^{-1}$  which resulted from Fano interference gradually dominate in the Raman spectra for the BDMD film with the increasing of B/C ratio. The electrochemical behaviors of BDMD film electrode show that the reversibility is improved for the diamond film electrode with high boron doping level. The increasing of boron atoms in diamond film significantly increases the electron transfer properties of the BDMD film electrode due to the enhanced conductivity. The glucose oxidation peak position and current density are dependent on the B/C ratio for the BDMD film electrodes. The BDMD film electrode with B/C ratio of 10 000 ppm demonstrates the highest sensitivity of  $96.88 \mu\text{A mM}^{-1} \text{cm}^{-2}$ , lowest detection limit of 0.018 mM and widest linear range of 0.1 to 5 mM in comparison with the other two diamond electrodes with B/C ratio of 8000 and 30 000 ppm, owing to the enhanced electrocatalytic activity, excellent electrical

conductivity and large active surface area. The appropriate boron concentration in diamond can improve the quality and electrochemical properties of the BDMD film. The glucose can be selectively detected in the presence of UA and AA in alkaline solution using the as-prepared BDMD film electrode.

## Acknowledgements

This work was financially supported by the Natural Science Foundation of Jiangsu Province of China (BK20141401), the Fundamental Research Funds for the Central Universities (30920130111019), and the Ningbo Science and Technology Innovation Team (2011B81001).

## References

- 1 M. Pumera, S. Sánchez, I. Ichinose and J. Tang, *Sens. Actuators, B*, 2007, **123**, 1195–1205.
- 2 W. Lohmann and U. Karst, *Anal. Chem.*, 2007, **79**, 6831–6839.
- 3 V. G. Gavalas, N. A. Chaniotakis and T. D. Gibson, *Biosens. Bioelectron.*, 1998, **13**, 1205–1211.
- 4 H. Yu, P. Li and J. Robertson, *Diamond Relat. Mater.*, 2011, **20**, 1020–1025.
- 5 J. Okuno, K. Maehashi, K. Matsumoto, K. Kerman, Y. Takamura and E. Tamiya, *Electrochem. Commun.*, 2007, **9**, 13–18.
- 6 Y. L. Zhou and J. F. Zhi, *Talanta*, 2009, **79**, 1189–1196.
- 7 N. J. Yang, W. Smirnov and C. E. Nebel, *Electrochem. Commun.*, 2013, **27**, 89–91.
- 8 C. Karuppiyah, S. Palanisamy, S. M. Chen, V. Veeramani and P. Periakaruppan, *Sens. Actuators, B*, 2014, **196**, 450456.
- 9 S. Singh and B. D. Gupta, *Sens. Actuators, B*, 2013, **177**, 589–595.
- 10 P. Si, Y. J. Huang, T. H. Wang and J. M. Ma, *RSC Adv.*, 2013, **3**, 3487–3502.
- 11 Y. X. Li, X. H. Niu, J. Tang, M. B. Lan and H. L. Zhao, *Electrochim. Acta*, 2014, **130**, 1–8.
- 12 Y. H. Kwak, D. S. Choi, Y. N. Kim, H. Kim, D. H. Yoon, S. S. Ahn, J. W. Yang, W. S. Yang and S. Seo, *Biosens. Bioelectron.*, 2012, **37**, 82–87.
- 13 S. Park, H. Boo and T. D. Chung, *Anal. Chim. Acta*, 2006, **556**, 46–57.
- 14 S. B. Bankar, M. V. Bule, R. S. Singhal and L. Ananthanarayan, *Biotechnol. Adv.*, 2009, **27**, 489–501.
- 15 M. Q. Guo, H. S. Hong, X. N. Tang, H. D. Fang and X. H. Xu, *Electrochim. Acta*, 2012, **63**, 1–8.
- 16 Y. J. Lee and J. Y. Park, *Sens. Actuators, B*, 2011, **155**, 134–139.
- 17 Y. Bai, Y. Sun and C. Sun, *Biosens. Bioelectron.*, 2008, **24**, 579–585.
- 18 S. Liu, B. Yu and T. Zhang, *Electrochim. Acta*, 2013, **102**, 104–107.
- 19 K. Tian, M. Prestgard and A. Tiwari, *Mater. Sci. Eng., C*, 2014, **41**, 100–118.
- 20 X. Li, Q. Y. Zhu, S. F. Tong, W. Wang and W. B. Song, *Sens. Actuators, B*, 2009, **136**, 444–450.
- 21 G. F. Wang, X. P. He, L. L. Wang, A. X. Gu, Y. Huang, B. Fang, B. Y. Geng and X. J. Zhang, *Microchim. Acta*, 2013, **180**, 161–186.

- 22 W. Gao, W. W. Tjiu, J. C. Wei and T. X. Liu, *Talanta*, 2014, **120**, 484–490.
- 23 L. M. Lu, L. Zhang, F. L. Qu, H. X. Lu, X. B. Zhang, Z. S. Wu, S. Y. Huan, Q. A. Wang, G. L. Shen and R. Q. Yu, *Biosens. Bioelectron.*, 2009, **25**, 218–223.
- 24 M. M. Liu, R. Liu and W. Chen, *Biosens. Bioelectron.*, 2013, **45**, 206–212.
- 25 Z. G. Zhu, L. G. Gancedo, C. Chen, X. R. Zhu, H. Q. Xie, A. J. Flewitt and W. I. Milne, *Sens. Actuators, B*, 2013, **178**, 586–592.
- 26 J. Luo, S. S. Jiang, H. Y. Zhang, J. Q. Jiang and X. Y. Liu, *Anal. Chim. Acta*, 2012, **709**, 47–53.
- 27 Y. S. Zou, L. L. He, Y. C. Zhang, X. Q. Shi, Z. X. Li, Y. L. Zhou, C. J. Tu, L. Gu and H. B. Zeng, *J. Appl. Electrochem.*, 2013, **43**, 911–917.
- 28 D. B. Luo, L. Z. Wu and J. F. Zhi, *ACS Nano*, 2009, **3**, 2121–2128.
- 29 T. Watanabe and Y. Einaga, *Biosens. Bioelectron.*, 2009, **24**, 2684–2689.
- 30 Q. Wang, P. Subramanian, M. S. Li, W. S. Yeap, K. Haenen, Y. Coffinier, R. Boukherroub and S. Szunerits, *Electrochem. Commun.*, 2013, **34**, 286–290.
- 31 J. T. Matsushima, W. M. Silva, A. F. Azevedo, M. R. Baldan and N. G. Ferreira, *Appl. Surf. Sci.*, 2009, **256**, 757–762.
- 32 N. Ndao, F. Zenia, A. Deneuve, M. Bernard and C. Lévy-Clément, *Diamond Relat. Mater.*, 2000, **9**, 1175.
- 33 R. Bogdanowicz, A. Fabiańska, L. Golunski, M. Sobaszek, M. Gnyba, J. Ryl, K. Darowicki, T. Ossowski, S. D. Janssens, K. Haenen and E. M. Siedlecka, *Diamond Relat. Mater.*, 2013, **39**, 82–88.
- 34 Y. S. Zou, Z. X. Li and H. Yang, *Surf. Eng.*, 2011, **294**, 294–299.
- 35 A. F. Azevedo, M. R. Baldan and N. G. Ferreira, *J. Phys. Chem. Solids*, 2013, **74**, 599–604.
- 36 D. Becker and K. Juttner, *New Diamond Front. Carbon Technol.*, 2003, **13**, 67–78.
- 37 J. W. Zhao, D. H. Wu and J. F. Zhi, *J. Electroanal. Chem.*, 2009, **626**, 98–102.
- 38 L. H. Li and W. D. Zhang, *Microchim. Acta*, 2018, **163**, 305–311.
- 39 S. L. Luo, F. Su, C. B. Liu, J. X. Li, R. H. Liu, Y. Xiao, Y. Li, X. N. Liu and Q. Y. Cai, *Talanta*, 2011, **86**, 157–163.
- 40 F. Xiao, Y. Q. Li, H. C. Gao, S. B. Ge and H. W. Duan, *Biosens. Bioelectron.*, 2013, **41**, 417–423.
- 41 M. Li, X. J. Bo, Z. C. Mu, Y. F. Zhang and L. P. Guo, *Sens. Actuators, B*, 2013, **177**, 589–595.
- 42 J. Zhao, L. M. Wei, C. H. Peng, Y. J. Su, Z. Yang, L. Y. Zhang, H. Wei and Y. F. Zhang, *Biosens. Bioelectron.*, 2013, **47**, 86–91.